PLOS COMPUTATIONAL BIOLOGY

RESEARCH ARTICLE

Multiscale model of integrin adhesion assembly

Tamara C. Bidone[1,2], Austin V. Skeeters[3], Patrick W. Oakes[3,4], Gregory A. Voth[1]*

1 Department of Chemistry, Institute for Biophysical Dynamics, and James Franck Institute, The University of Chicago, Chicago, Illinois, United States of America, **2** Department of Bioengineering and Scientific Computing and Imaging Institute, University of Utah, Salt Lake City, Utah, United States of America, **3** Department of Physics & Astronomy, University of Rochester, Rochester, New York, United States of America, **4** Department of Biology, University of Rochester, Rochester, New York, United States of America

* gavoth@uchicago.edu

OPEN ACCESS

Citation: Bidone TC, Skeeters AV, Oakes PW, Voth GA (2019) Multiscale model of integrin adhesion assembly. PLoS Comput Biol 15(6): e1007077. https://doi.org/10.1371/journal.pcbi.1007077

Editor: Qiang Cui, Boston University, UNITED STATES

Received: February 6, 2019

Accepted: May 8, 2019

Published: June 4, 2019

Data Availability Statement: The code used to perform the simulations is available at https://github.com/tamarabidone/IntegrinClustering.

Funding: This research was supported by the Department of Defense Army Research Office through MURI grant W911NF1410403. It was also partially supported by the University Chicago Materials Research Science and Engineering Centre, which is funded by the National Science Foundation under award number DMR-1420709. Computer time was provided by the University of Utah Research Computing Centre. The funders had no role in study design, data collection and

Abstract

The ability of adherent cells to form adhesions is critical to numerous phases of their physiology. The assembly of adhesions is mediated by several types of integrins. These integrins differ in physical properties, including rate of diffusion on the plasma membrane, rapidity of changing conformation from bent to extended, affinity for extracellular matrix ligands, and lifetimes of their ligand-bound states. However, the way in which nanoscale physical properties of integrins ensure proper adhesion assembly remains elusive. We observe experimentally that both β-1 and β-3 integrins localize in nascent adhesions at the cell leading edge. In order to understand how different nanoscale parameters of β-1 and β-3 integrins mediate proper adhesion assembly, we therefore develop a coarse-grained computational model. Results from the model demonstrate that morphology and distribution of nascent adhesions depend on ligand binding affinity and strength of pairwise interactions. Organization of nascent adhesions depends on the relative amounts of integrins with different bond kinetics. Moreover, the model shows that the architecture of an actin filament network does not perturb the total amount of integrin clustering and ligand binding; however, only bundled actin architectures favor adhesion stability and ultimately maturation. Together, our results support the view that cells can finely tune the expression of different integrin types to determine both structural and dynamic properties of adhesions.

Author summary

Integrin-mediated cell adhesions to the extracellular environment contribute to various cell activities and provide cells with vital environmental cues. Cell adhesions are complex structures that emerge from a number of molecular and macromolecular interactions between integrins and cytoplasmic proteins, between integrins and extracellular ligands, and between integrins themselves. How the combination of these interactions regulate adhesions formation remains poorly understood because of limitations in experimental approaches and numerical methods. Here, we develop a multiscale model of adhesion assembly that treats individual integrins and elements from both the cytoplasm and the

analysis, decision to publish, or preparation of the manuscript.

Competing interests: The authors have declared that no competing interests exist.

extracellular environment as single coarse-grained (CG) point particles, thus simplifying the description of the main macromolecular components of adhesions. The CG model implements sequential interactions and dependencies between the components and ultimately allows one to characterize various regimes of adhesions formation based on experimentally detected parameters. The results reconcile a number of independent experimental observations and provide important insights into the molecular basis of adhesion assembly from various integrin types.

Introduction

As the linker between cytoskeletal adhesion proteins and extracellular matrix ligands, integrins play a vital role in the formation of adhesions and profoundly influence different phases of cell physiology, such as spreading, differentiation, changes in shape, migration and stiffness sensing [1–5].

Integrins are large heterodimeric receptors, with a globular headpiece projecting more than 20 nm from the cell membrane, two transmembrane helices, and two short cytoplasmic tails that bind cytoskeleton adhesion proteins (see Fig 1A). In order to form adhesions, integrins undergo lateral diffusion on the cell membrane, switch conformation from bent to extended, and change chemical affinity for extracellular matrix (ECM) ligands, E_{IL}. Integrins also assemble laterally, owing to interactions with talin [6,7], kindlin [8], or glycocalyx [9], and can grow nascent adhesions into mature adhesions [10–12]. Integrin diffusion, activation, ligand binding, and clustering occur at the individual protein scale, but their effects can also be reflected on the cellular scale, resulting in a multiscale biological process. Simulations of adhesion assembly based on all-atom approaches are too detailed and computationally demanding to capture adhesion formation from multiple integrins. Instead, highly coarse-grained, CG, approaches based on Brownian Dynamics can condense the description of individual proteins into a few interacting CG "beads" that can recapitulate the emergent dynamics of complex biological systems from its individual components (see, e.g., Refs [13–17] for the example of cytoskeleton networks).

Nascent adhesions are complex biological systems that form near the leading edge of protruding cells, appearing as spots of about 0.1 μm in diameter, with lifetimes of 2–10 min (Fig 1B) [18–22]. Unfortunately, the small size and short lifetime of nascent adhesions have made it challenging to study them experimentally. Among 24 different integrin isoforms, the $\alpha_v\beta_3$ and $\alpha_5\beta_1$ integrins, have important, but potentially separate roles in the assembly of adhesions and the physiology of many cell types [23–32]. Nanoscale differences in physical properties between $\alpha_v\beta_3$ and $\alpha_5\beta_1$ integrins can determine how nascent adhesions assemble [33], their organization [34–36], transmitted traction [37] and lifetime [38], on account of their different properties. For example, it has been reported that the rate of integrin activation, k_a, determines the number of integrins per adhesion [21,39], while lateral clustering, or avidity, E_{II}, increases the size of individual adhesions [40–42].

Single-protein tracking experiments combined with super-resolution microscopy and computational methods have helped extract physical properties of different integrin types. β-1 and β-3 integrins were found to have diffusion coefficients of 0.1 and 0.3 $\mu m^2/s$, respectively [43]. β-1 integrins also maintain their active conformation longer than β-3 integrins. Free-energy energy differences between active and inactive states revealed activation rates for β-3 integrins about 10-fold higher that β-1 integrins [44,45]. The intrinsic ligand binding affinity, E_{IL}, of β-1 integrins for soluble fibronectin is about 10–50 fold higher than β-3 integrins, spanning an overall range for the two integrins of 3–9 k_BT [46]. β-1 integrins display a catch bond

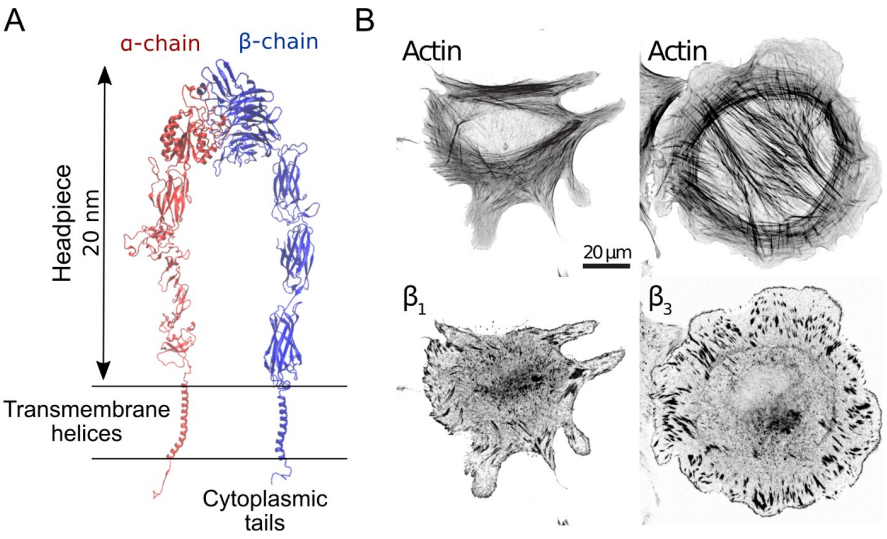

Fig 1. Both β-1 and β-3 integrins localize at the cell periphery, where nascent adhesions assemble. (A) Cartoon representation of active, fully extended $\alpha_{IIb}\beta_3$ integrin, which is closely related to $\alpha_v\beta_3$ [82]. (B) Representative images of human foreskin fibroblasts (HFF) fixed after 60 minutes of spreading on fibronectin coated glass coverslips and immunostained for actin and either β-1 or β-3 integrins.

https://doi.org/10.1371/journal.pcbi.1007077.g001

and adhesion strength-reinforcing behavior and are stationary within adhesions [47–49]. β-3 integrins, on the other hand, rapidly transit from closed to open conformations, break their bonds from ligands more easily under modicum tensions, and undergo rearward movements within adhesions [26,38]. How these differences in diffusion, rate of activation, ligand binding affinity, and bond dynamics reflect on the assembly of nascent adhesions and on the probability of adhesion maturation remains elusive.

In this paper, we show that mixed populations of β-1 and β-3 integrins localize to both nascent and mature adhesions, suggesting that there could be important interactions between the two types of integrins. To address this question, we have developed a highly CG model of adhesion formation, based on Brownian Dynamics (Fig 2) and study how nanoscale physical properties of different types of integrins interplay in the assembly of nascent adhesions. The CG model treats individual integrins as point particles within an implicit cell membrane and includes actin filaments as explicit semiflexible polymers (Fig 2A). By incorporating nanoscale physical properties of individual integrins, sequential interactions and feedback mechanisms between integrin, ligands and actin filaments (Fig 2B–2D), the model is used to characterize the formation of micrometer-size adhesions at the cell periphery in a multiscale fashion. Our calculations show that integrins with high E_{IL} and enhanced bond lifetimes, such as β-1 integrins, facilitate ligand binding, transmission of traction stress, and engagement of actin networks. By contrast, integrins with low E_{IL} and lower ligand bond lifetimes, such as β-3 integrins, are correlated with clustering, repeated cycles of diffusion and immobilization, and weak engagement of actin filaments. The architecture of actin filaments does not impact the amount of ligand binding and integrin clustering, but determines the probability of adhesions maturation, consistent with previous experimental findings [50]. Collectively, our data reveal important insights into adhesions assembly that are currently very challenging to obtain experimentally. The data supports the general view that cells, by controlling physical nanoscale properties of integrins via expression of specific types, can regulate structural, dynamical, and mechanical properties of adhesions.

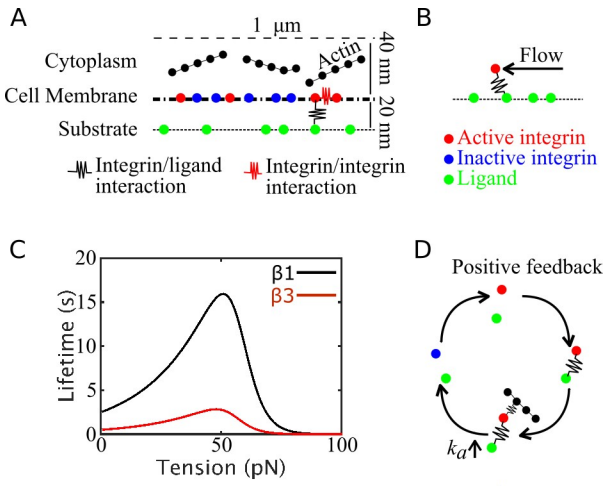

Fig 2. Schematic illustration of the model system. (A) Side view of the computational domain, where single-point, two-state integrin particles diffuse and assemble laterally. Upon activation (from blue to red), integrins can establish interactions (black spring) with ligands (green particles) and other active integrins (red springs). (B) Schematics of the system with actin flow: a force mimicking actin flow is exerted on ligand-bound integrins, parallel to the substrate, and builds tension on the integrin/ligand bond. (C) Lifetime versus tension curves of catch bonds used to mimic β-1 (black) and β-3 (red) integrins. (D) Schematic illustration of the positive feedback between actin filament binding and integrin activation. Once an integrin particle is bound to a ligand, it can establish interactions with actin. Upon binding actin, its activation rate increases. Upon deactivating and unbinding, its propensity to become active again increases, leading to increased probability of binding new ligands and actin filaments. This results in a positive feedback between ligand binding and engaging the actin cytoskeleton.

https://doi.org/10.1371/journal.pcbi.1007077.g002

Results

Both β-1 and β-3 integrins localize in nascent and mature adhesions

Motivated by our recent work on integrin catch-bonds regulating cellular stiffness sensing [5], we sought to investigate how interactions between different integrins could affect adhesion formation. Immunostaining in Human Foreskin Fibroblasts (HFF) for actin and either β-1 or β-3 integrins revealed that both types of integrins localize in nascent adhesions at the cell leading edge and in mature adhesions at the end of actin stress fibers (Fig 1B). This suggests that potential interactions between the different adhesion populations could be important during adhesion formation. To address this question, we developed a computational model to investigate how the nanoscale properties of different integrins affect adhesion formation and stability.

Integrin clustering decreases with ligand binding affinity

Since β-1 and β-3 integrins differ in ligand binding affinity, E_{IL}, and strength of pairwise interactions, E_{II} [44,45], we use the CG model to test how variations in E_{II} and E_{IL} impact adhesion assembly in terms of the amount of integrin clustering, ligand binding, and spatial arrangement of adhesions. Different morphological arrangements of integrin adhesions are detected (Fig 3A–3C). For high E_{II} and low E_{IL}, clustering is promoted (Fig 3D), but only a few integrins are bound to ligands (Fig 3E), resulting in few large integrin clusters (Fig 3A). Conversely, for low E_{II} and high E_{IL}, only a few integrins cluster (Fig 3D) while ligand-binding is promoted (Fig 3E), resulting in many ligand-bound integrins and few small integrin clusters (Fig 3B). When E_{II} and E_{IL} have intermediate values, a mix of big clusters of integrins that are weakly bound to the substrate and smaller, ligand-bound clusters co-exist (Fig 3C). By systematically varying E_{II} and E_{IL}, morphological regions differing in size and

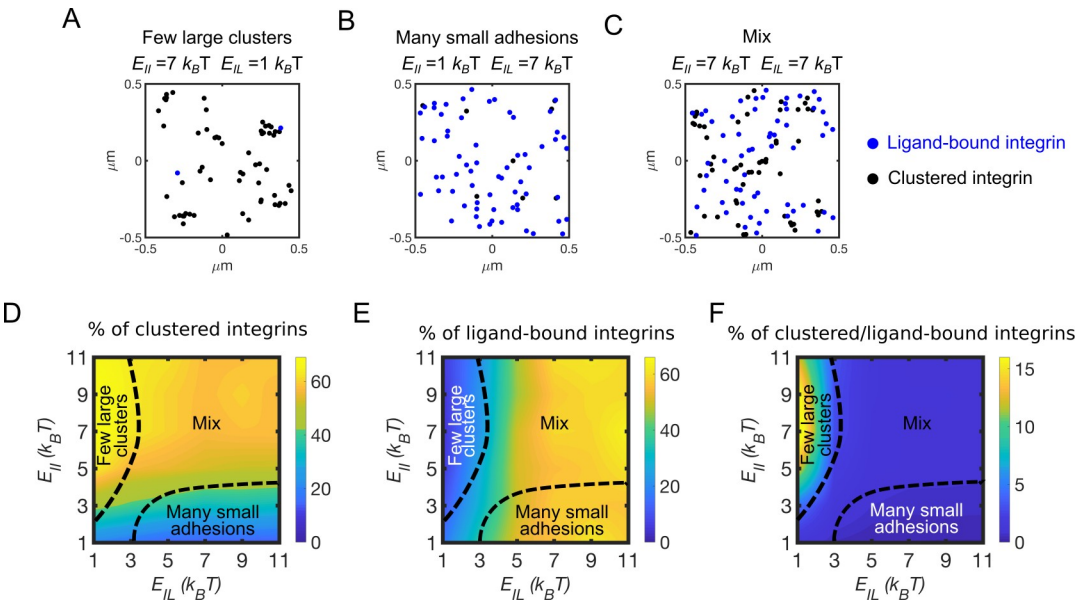

Fig 3. Integrin affinity and avidity determine clustering and ligand binding. (A) Configuration of clustered integrins (black circles) and ligand-bound integrins (blue circles) at a time point between 80–100 s of simulations, using E_{II} = 7 k_BT and E_{IL} = 1 k_BT. (B) Configuration of clustered integrins (black circles) and ligand-bound integrins (blue circles) at a time point between 80–100 s of simulations, using E_{II} = 1 k_BT and E_{IL} = 7 k_BT. (C) Configuration of clustered integrins (black circles) and ligand-bound integrins (blue circles) at a time point between 80–100 s of simulations, using E_{II} = 7 k_BT and E_{IL} = 7 k_BT. (D) Average percentage of clustered integrins relative to total integrins, by varying E_{IL} and E_{II}. (E) Average percentage of ligand-bound integrins relative to total integrins, by varying E_{IL} and E_{II}. (F) Fraction between clustered and ligand-bound integrins, by varying E_{IL} and E_{II}. This indicates the amount of clustered integrins per ligand-bound integrin. All data are computed between 100–130 s of simulations, from four independent runs.

https://doi.org/10.1371/journal.pcbi.1007077.g003

number of ligand-bound integrins versus clusters were precisely identified. A region of few large clusters exists for E_{II} >3 k_BT and E_{IL} < 3 k_BT; a region of many small adhesions exists for E_{II} < 3 k_BT and E_{IL} > 3 k_BT; the rest of the parameter space shows co-existence of intermediate-size clusters and ligand-bound integrins (Fig 3D–3E). The fraction of ligand-bound integrins increases with E_{IL} and is independent from E_{II}. (Fig 3E). By contrast, clustering is not independent from E_{IL} and is promoted when E_{IL} is low (Fig 3D). In the model, when active, integrins can bind free ligands and cluster, when in close proximity of a ligand or another active integrin, respectively. Since the number of ligands is higher than the number of integrins, the probability for an integrin to find a free ligand is higher than that of finding an active integrin. Therefore, clustering increases less with E_{II} when E_{IL} is high than when E_{IL} is low (Fig 3D). This indicates that integrin clustering and ligand binding are competing mechanisms.

Together, our results show that different arrangements of nascent adhesions can be achieved depending on E_{II} and E_{IL}. When we use high E_{II} and low E_{IL}, as for β-3 integrins, clustering is enhanced, and ligand binding reduced; when we use high E_{IL} and low E_{II}, as for β-1 integrins, clustering is reduced, and ligand-binding promoted. Thus, the competition between clustering and ligand binding can be determined by the integrin type. However, β-1 and β-3 integrins also differ in their rates of activation, which can lead to differences in this competition, by promoting clustering at high E_{IL}. Therefore, we next aimed to understand how activation rates, combined with variations in E_{II} and E_{IL}, impact clustering and ligand binding.

Rate of integrin activation increases clustering and ligand binding

Competition between integrin clustering and ligand binding can be determined by the difference in activation rate between β-1 and β-3 integrins. By varying k_a from 0.005 s^{-1} to 0.5 s^{-1}, our model shows that both clustering and ligand binding are promoted (Fig 4A and 4B). Using E_{II} = 5 k_BT and varying E_{IL} from 3 k_BT to 11 k_BT, clustering is independent from E_{IL} (Fig 4A), while overall ligand binding increases with E_{IL} (Fig 4B). Clustering is mostly set by the strength of pairwise interactions between integrins, E_{II}. It can be promoted by low E_{IL}, and high k_a, leading to a higher number of integrins able to diffuse and cluster (Fig 4A). Ligand binding is proportional to E_{IL} at all k_a. In experiments, variations in integrin activation rate are tied to variations in ligand binding affinity, making it unclear whether it is k_a or E_{IL} that determines organization of nascent adhesions. Our model shows that the rate of integrin activation set the level of the competition between ligand binding affinity and strength of pairwise interactions (Fig 4A).

Experimentally, Mn^{2+} or antibodies are typically used to modulate ligand binding affinity [51–54]. Both of these approaches, however, not only increase ligand binding affinity, but also the lifetime of the ligand bond. The increase of the ligand bond lifetime can be formally represented using a catch-bonds [55], where ligand unbinding rates decrease under tension and promotes stress transmission from the adhesions [56]. Therefore, we next used the model to test how variations in catch bond kinetics, combined with differences in the relative amount of β-1 and β-3 integrins, modulate ligand binding and stress transmission.

Distribution of tension on integrins depends on bond dynamics

Since nascent adhesions transmit tension between the cytoskeleton and the ECM, we next asked how mixing integrins with different load-dependent bond kinetics impacts ligand binding and transmitted tension. The β-1 and β-3 integrins both behave as catch bonds that differ for unloaded and maximum lifetimes (Fig 2C). In the model, an increase in the percentage of β-1 integrins while keeping the rest as β-3 integrins, increases ligand binding from about 5% to 35% when using actin flow speeds below 15 nm/s (Fig 5A). The percentage of ligand-bound integrins is in direct proportion to the amount of β-1 integrins (Fig 5A). At actin flow speeds below 15 nm/s, traction stress and flow rate are positively correlated, while at higher flows they are inversely correlated (Fig 5B), in agreement with previous findings [60, 61]. Interestingly, variations in the relative fractions of the two integrin types do not affect the average tension on each integrin-ligand bond (Fig 5B). Below 10 nm/s actin flow, the minimum separation between ligand-bound integrins decreases from about 120 to 10 nm by increasing the fraction

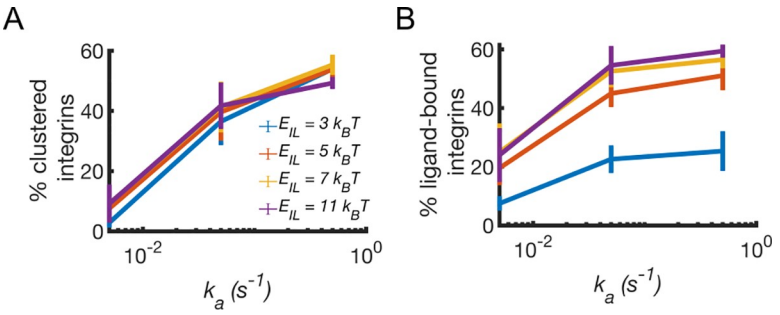

Fig 4. Integrin activation rate enhances clustering and ligand binding. (A) Average percentage of clustered integrins as a function of activation rate, k_a, by varying ligand binding affinity, E_{IL}, and keeping E_{II} = 5 k_BT. (B) Corresponding average percentage of ligand-bound integrins. Data are computed between 10–200 s of simulations from three independent runs. Error bars indicate standard deviation from the mean.

https://doi.org/10.1371/journal.pcbi.1007077.g004

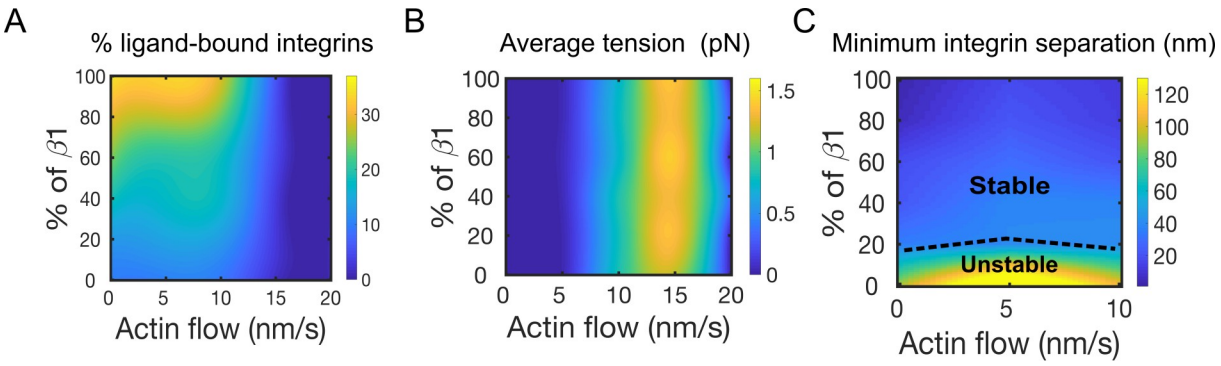

Fig 5. Amounts of β-1 and β-3 integrins determine ligand binding, traction stress, and adhesion stability. (A) Percentage of ligand-bound integrins by varying fraction of β-1 in a system of β-3 integrins, as a function of actin flow speed. (B) Average tension per integrin varying actin flow speed and percentage of simulated β-1 in a system of β-3 integrins. (C) Average distance between nearest ligand-bound integrins, without distinction between β-1 and β-3 integrins. Represented are regions of unstable and stable adhesions, depending upon the minimum spatial separation between any integrin type. Data are computed as averages between 1–120 s of simulations.

https://doi.org/10.1371/journal.pcbi.1007077.g005

of β-1 integrins (Fig 4C). Stable adhesions, with minimum separation between ligand-bound integrins of 70nm, form with at least 20% β-1 integrins (Fig 5C). Together, our results show that the relative fractions of β-1 and β-3 integrins cooperate with actin flow to determine ligand binding and adhesion stability.

Actin architecture does not impact integrin clustering and ligand binding, but changes the physical organization of integrins in adhesions

Interactions of adhesions with a cytoskeleton network play important role in several cell activities, including spreading and migration. The actin cytoskeleton exists in different architectures, depending on the cell location and function. Therefore, we next considered how the architecture of the actin cytoskeleton can impact the formation of adhesions. We incorporated in the model explicit actin filaments, using random, crisscrossed, and bundled architectures (Fig 6A–6C). The model assumes that ligand-bound integrins can interact with actin filaments, and that binding to actin increases integrin activation rate, as detected experimentally [63, 64]. Increasing the fraction of β-1 integrins, ligand binding increases independent of network architecture (Fig 6D). By contrast, integrin clustering remains at about 20–30% when a percentage of β-3 integrins is used. When only β-1 integrins are used, integrin clustering decreases of about 3-fold, independent from network architecture (Fig 6E). The number of ligand-bound integrins with a separation less than 70 nm is enhanced using a bundled network architecture (Fig 6F). This suggests that the probability of adhesion stability and ultimately maturation is higher with bundled architectures relative to both crisscrossed and random distributions of actin filaments (Fig 6F).

Collectively, our results indicate that the architecture of the actin cytoskeleton does not modulate the amount of ligand binding and integrin clustering. However, actin network architecture determines the physical distribution of ligand-bound integrins in adhesions, with bundled actin filaments increasing the probability of adhesion stability, consistent with previous experimental observations [50].

Discussion

Since our experiments show that different integrin types exist in nascent and mature adhesions (Fig 1B), a computational model is here developed in order to understand if differences in

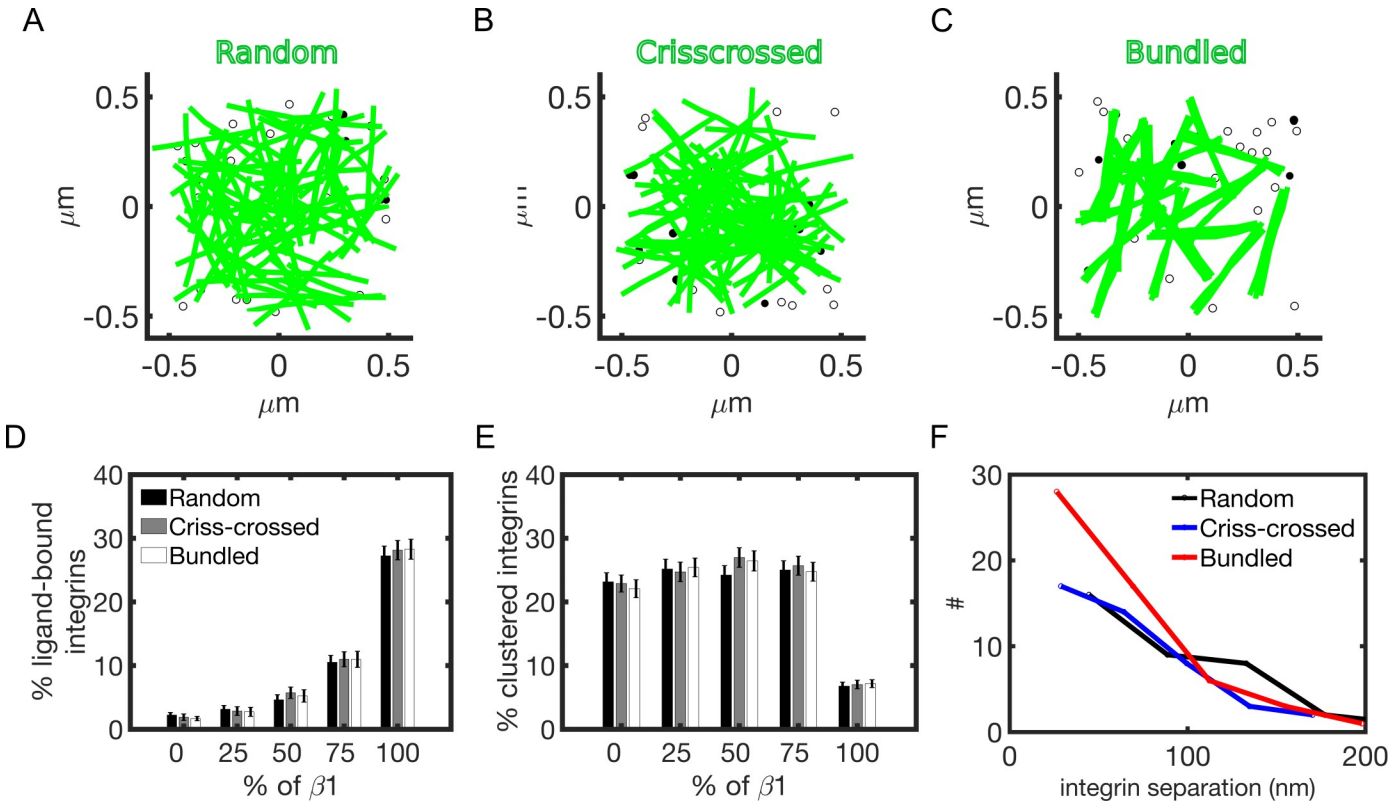

Fig 6. Actin architecture does not impact integrin clustering and ligand binding but changes the physical distribution of integrins in adhesions. (A-C) Snapshots from the simulations: random, crisscrossed and bundled actin networks above a layer of integrins. Filled circles indicate clustered integrins; empty circles indicate ligand-bound integrins. (D) Average percentage of ligand-bound integrins with respect to increasing amount of β-1 integrins (using $E_{IL} = E_{II} = 9\ k_BT$) at varying actin architectures. (E) Corresponding percentage of clustered integrins. (F) Distribution of average nearest neighbor distances between ligand-bound integrins using 50% β-1 integrins at varying actin architectures. Results are computed as averages between 20–30 s of simulation.

https://doi.org/10.1371/journal.pcbi.1007077.g006

nanoscale physical properties of integrins reflect on adhesions. This is largely untested by experimental approaches because it is very challenging to simultaneously distinguish between integrin types and isolate their nanoscale physical properties. The model is used to study how ligand binding affinity, rate of integrin activation, strength of pairwise interactions, bond kinetics, as well as the architecture of a network of actin filaments modulate integrin organization in adhesions and stress transmission. Our results collectively show that ligand binding and integrin clustering are competing mechanisms and that bundled actin networks favor adhesions stability, and ultimately maturation.

The model is developed through three consecutive stages of increasing complexity: (*i*) simulations of single-point integrins diffusing on a quasi-2D surface and switching between active and inactive states, binding ligands, and interacting laterally; (*ii*) incorporation of an implicit actin flow and integrin/ligand catch bonds kinetics; (*iii*) binding of integrins to semi-flexible actin filaments in either random, bundled, or crisscrossed architectures. At all stages, we distinguish between β-1 and β-3 integrins, by using either exact, experimentally detected physical parameters, realistic fold differences between the two, or estimates from previous free energy calculations.

For high E_{IL}, many active integrins bind ligands and the fraction of integrins that can diffuse, and cluster, is reduced (Fig 3D–3E). Accordingly, this happens when the fraction of β-1 integrins is higher than that of β-3 integrins (Fig 5A), since β-1 integrins have higher ligand-

binding affinity than β-3 integrins. By contrast, with many free diffusing integrins that have low E_{IL}, and are less likely to bind ligands, the fraction of integrins that can encounter each other, and cluster is enhanced and reduces ligand binding (Fig 3D–3E). This happens when the fraction of β-3 integrins is higher than that of β-1 integrins (Fig 5A) and also results from the higher diffusion coefficient of β-3 integrins with respect to β-1 integrins [43,44]. The result that ligand binding and integrin clustering are competing mechanisms is consistent with a kinetic Monte Carlo model showing that thermodynamics of ligand binding and dynamics of integrin clustering interplay [46]. Our model reproduces this competing process over the same range of ligand binding affinities and strength of pairwise interactions.

The molecular mechanisms resulting in integrin lateral clustering remain controversial. However, several lines of evidence have suggested that β -3 integrins assemble clusters more easily than β-1 integrins. For example, activation of β -3 integrins induces formation of clusters with recruitment of talin [7], while β-1 integrins require recruitment of many more signaling components in order to form clusters, such as FAK [57]. β-3 integrins cluster in response to talin binding without a concomitant increase in affinity [24], while β-1 integrins cluster only when extended [58]. Moreover, previous studies in U2OS cells showed that β-3 integrins cluster on both β-3 and β-1 integrin ligands, while β-1 integrin clusters are present in adhesions only on β-1 ligands [59]. Our result that β-1 integrins are correlated with ligand-binding while β-3 integrins are mostly responsible for clustering is consistent with the observation that clusters of β-1 integrins are present only on β-1 ligands, possibly because, in this case, ligand binding and not pairwise interactions facilitate adhesions assembly. Further evidence that β-3 integrins assemble more easily than β-1 integrins is provided by the reported spatial and functional segregation of the two integrin types. β-1 integrins translocate from the cell periphery to the cell center to withstand higher tensions, whereas β -3 integrins remain at the cell edges to do mechanosensitive activities via dynamic breakage and formation of multiple bonds with the substrate and with one another [38].

Our model also shows that the number of integrins per cluster, computed as the fraction of clustered versus ligand bound integrins, is in the range of 2–15 particles, depending on E_{II} and E_{IL} (Fig 3F). This value is comparable to the experimentally estimated number of integrins in nascent adhesions, between 5–7 [10]. By varying ligand density in the model, the ratio between clustered and ligand bound integrin particles does not vary significantly (S1 Fig), suggesting that the average number of integrins per cluster in nascent adhesions is not modulated by ligand concentration, consistent with previous experimental observations [10].

In the presence of actin flow, the fraction of β-1 integrins is positively correlated with ligand binding (Fig 5A). Above a threshold actin flow, however, ligand binding is almost suppressed, independent from relative amounts of β-1 and β -3 integrins (Fig 5A), because of faster ligand unbinding from both integrins. This reduction in bound ligands corresponds to a drop in the average tension per integrin upon increasing actin flow (Fig 5B). The biphasic response of tension to actin flow was previously observed experimentally [60] and is consistent with models of adhesion clutch assembly and rigidity sensing [61]. By increasing the fraction of β-1 integrins, a reduction of lateral integrin spacing is observed with our model (Fig 5C). Previous studies on the lateral separation of integrins in adhesions reported that a minimum spacing of 70 nm is required to form stable adhesions [62]. This value corresponds in the model to a minimum of 20% β-1 integrins (Fig 5B). This value represents a prediction from our CG model that can be experimentally tested in the future. When only β-3 integrins are used in the model, their lateral separation, upon binding ligands, is about 120 nm (Fig 5C), supporting the notion that β-1 integrins are needed to form stable adhesions. This is consistent with the fast binding/unbinding dynamics of β-3 integrins previously observed in experiments [28].

By incorporating a positive feedback between actin filament engagement and integrin activation, as observed in [63,64], the competition between clustering and ligand binding is maintained in all actin architectures (Fig 6D–6E). This positive feedback represents the functional link between cytoskeleton and adhesions, where an increase in the probability of ligand binding results from binding actin, via an inside-out pathway [12,65]. Our model shows that the number of ligand-bound integrins with an average separation below 70 nm is enhanced with a bundled architecture (Fig 6F), suggesting that this configuration favors adhesion stability, and ultimately maturation [50]. When integrins bind a bundled network, they are likely to re-bind in close proximity because bundled filament architectures present filaments that are spatially closer than filaments of crisscrossed or random networks, forming a spatial trap for the receptors. Of interest for future studies is mimicking conditions of actin filament turnover, in order to understand how a dynamic cytoskeleton can interplay with integrin mixing in forming nascent adhesions. This will help understanding outside-in pathways, where, for example, adhesions formation modulates actin filaments polymerization. A further extension of the model will incorporate dynamic ligands, interconnected by a fibrous extracellular matrix that deform under tension. We will study how adhesions formation can change ligand localization and how this, in turns, affects adhesions morphology.

Previous computational studies of integrin dynamics range from all-atom simulations and enhanced sampling methods for understanding integrin activation at the level of individual molecules [66–68], to lower resolution coarse-grained [61,69–74], lattice-based [75,76], diffusion-reaction algorithms [77] and theoretical models [78] for multiple integrins. With respect to the previous lower resolution models of multiple integrins, our new model allows us to directly incorporate properties of different integrin types, as detected experimentally (Fig 1B). The particle-based implementation scheme of our model is similar to that of other software for modeling the cytoskeleton, such as Cytosim [79] and Medyan [80]. However, important differences exist. In contrast to Cytosim, an explicit implementation scheme is used here because our time step, combined with the limited number of simulated particles (a few hundreds), allows us to achieve time scales of a few minutes, that are relevant for adhesion assembly, without excessive computational cost. In addition, in contrast to Medyan, our model does not have a scheme for solving stochastic reaction-diffusion equations, but instead focuses on the mechanics of particle interactions and displacements under deterministic and Brownian forces.

To conclude, with our highly coarse-grained model based on Brownian Dynamics, we extend the scope of previous theoretical and computational studies of integrin-based adhesions formation, by testing how differences in nanoscale properties of β-1 and β-3 integrins impact ligand binding, clustering and transmission of traction stress. By coupling physical parameters (such as diffusivity) together with chemical (i.e., affinity and receptor pairwise interactions) and mechanical (bond kinetics) parameters, and by using an explicit actin cytoskeleton, our model shows that nascent adhesions assembly can be finely tuned by differences in nanoscale physical properties of integrins. The CG model ultimately demonstrates that nanoscale differences in integrin dynamics are sufficient to determine ligand binding and integrin clustering. By incorporating dynamics of individual integrins in an explicit way, our model provides results that are consistent with a number of previous independent experimental observations, revealing important insight into the molecular origins of adhesion organization and mechanics. Taken together, our modeling results support the general view that a cell can control integrin expression to determine morphological and dynamic properties of adhesions.

Methods

In order to characterize how nanoscale physical properties of integrins impact the assembly of nascent adhesions, we developed a highly coarse-grained computational model based on Brownian Dynamics. The model is agent-based in the way sequential dependencies regulate interactions between integrin/ligand, integrin/integrin, and integrin/actin. Integrins, ligands, and actin filaments are explicit particles, while the cell membrane is implicit. Solvent molecules mimicking cytoplasmic effects are replaced by stochastic forces, depending on cytoplasmic viscosity. Inactive integrins diffuse and, when active, can bind ligands and interact laterally. When integrins are bound to ligands, they can engage actin filaments. The interaction between integrins and actin filaments locally increases integrin activation rate, ultimately resulting in a positive feedback between actin binding and ligand binding [61,81].

In order to distinguish between β-1 and β-3 integrins, we examine the effect of varying integrin activation rates, motility, ligand binding affinity, clustering, and bond kinetics (Fig 2A–2C). By varying the relative amounts of β-1 and β-3 integrins, we analyze fractions of ligand-bound integrins, clustered integrins, and average tension on integrin-ligand bonds (Figs 3–5). Moreover, we study the effect of different actin filaments architecture on adhesions morphology (Fig 6).

The model is an extension of our mechanosensing model [5] but differs from it in several ways. First, each integrin exists in either active or inactive state, determined by activation and deactivation rates. Second, the model incorporates tunable parameters for integrin physical properties, allowing us to discriminate between integrin types. Third, explicit semiflexible actin filaments are included.

Computational domain

The computational domain includes two systems: a square bottom surface, of 1 μm per side, and a rectangular 3D domain above the surface, with dimensions 1 x 1 x 0.04 μm (Fig 2A). The bottom surface mimics the substrate; the lower side of the rectangular domain mimics the ventral cell membrane above the substrate, while its inside space represents a 40 nm thick cytoplasmic region where actin filaments diffuse beyond the ventral membrane (Fig 2A). The cell membrane is separated from the substrate by 20 nm, a dimension characteristic of active integrin headpiece extension (Fig 1A) [82]. Within the cell membrane, integrins diffuse in quasi-2D and are restrained in the vertical direction by a weak harmonic potential with spring constant 100 pN/μm, mimicking membrane vertical friction. In the cytoplasmic region, a repulsive boundary is used on the top surface, to avoid filaments crossing the boundary. Periodic boundary conditions are applied on all lateral sides of the domain, in order to avoid finite size effects.

Integrin and ligands representation

The model considers a given number of ligands on the substrate, randomly distributed and fixed in space. We use a ligand density of 1000#/μm^2, of the same order of that used in a previous model of adhesions assembly [72]. Integrin density on the cell membrane is ~100#/μm^2 [5]. Integrins are single-point particles, that are initially randomly distributed and diffuse over the course of the simulations. Integrin diffusion coefficient is $D = 0.1\ \mu m^2/s$ for β-1 integrins and $D = 0.3\ \mu m^2/s$ for β-3 integrins [43]. Introducing volume exclusion effects between integrins, in the form of a weak repulsion between nearby particles (1 pN force), does not change the fraction of ligand-bound integrins, their average separation, the mean tension per integrin and its distribution (see S2A–S2D Fig). Increasing the magnitude of this repulsion (10 pN), however, affect the average separation of integrins (S2E–S2F Fig).

Actin filament representation

Semiflexible polymers represent actin filaments as spherical particles connected by harmonic interactions. Filaments have fixed length of 0.5 μm, corresponding to 6 beads separated by 0.1 μm equilibrium distance. The model of actin filaments is explained in detail in [83]. Actin filament beads are subjected to both stochastic and deterministic forces. Stochastic forces on the *i*-th bead are random in direction and magnitude in order to mimic thermal fluctuations and satisfy the fluctuation-dissipation theorem:

$$\langle F_i^{stochastic} \cdot F_i^{stochastic^T} \rangle_{\alpha,\beta} = 2(k_B T \mu / dt) \hat{I}_{\alpha,\beta} \quad (1)$$

with $\hat{I}_{\alpha,\beta}$ being the second-order unit tensor [84] and μ being a friction coefficient equal in three directions.

Deterministic contributions come from bending and extensional forces on the filament beads. The bending force is computed as:

$$F_i^{bend} = \frac{-dE^{spring}}{d\boldsymbol{r}_i} = \frac{k_B T l_p}{l_0} \sum_{j=1}^{N-1} \frac{d(\boldsymbol{t}_j \cdot \boldsymbol{t}_{j-1})}{d\boldsymbol{r}_i} \quad (2)$$

where l_p = 10 μm is actin filament the persistence length, N is the number of beads in a filament (N = 6) and $t_i = \frac{(r_{j+1} - r_j)}{|r_{j+1} - r_j|}$.

The extensional force on filaments beads is computed as:

$$F_i^{extension} = \frac{-dE^{extension}}{d\boldsymbol{r}_i} = \frac{k}{2} \sum_{j=1}^{N-1} \frac{d(|\boldsymbol{r}_{j+1} - \boldsymbol{r}_j| - l_0)^2}{d\boldsymbol{r}} \quad (3)$$

where l_0 is the equilibrium length of 0.1 μm, k is the spring constant of 100 pN/μm.

Each spherical particle of a filament represents a binding site for integrin and each binding site can interact with multiple integrins.

Agent-based algorithm

In order to mimic hierarchical formation of nascent adhesions [10], the algorithm incorporates sequential interactions between integrins, ligands and actin filaments. First, we simulate a system composed of only integrins and ligands, in order to explore the ways in which integrins cluster and bind ligands in an actin-independent way. Then, we add actin filaments and study the effect of actin network architecture on adhesions formation.

Integrins switch between inactive and active states, with rates of activation and deactivation k_a = 0.5 s^{-1} and k_d = 0.0001 s^{-1}, of the same orders of those previously estimated [44,45,72]. Activation probability corresponds to $P_a = k_a dt$, with time-step dt = 0.0001 s, as the time of the smallest simulated phenomena. This large time-step is allowed because the extensional stiffness of actin filaments, 100 pN/μm, is smaller than the real actin filaments stiffness, of about 400 pN/nm [85]. Upon activation, integrins can interact with free ligands, using a harmonic potential (with equilibrium separation 20 nm and spring constant 1 pN/μm), and cluster with other active integrins, depending on relative distances. Ligand binding occurs within a threshold distance of 20 nm, which reflects the extension of the open conformation of $\alpha_{IIb}\beta_3$ integrin away from the membrane [82]. Each integrin can bind only one ligand, and each ligand can bind only one integrin, mimicking binding sites specificity. Clustering occurs below a threshold of 30 nm, a value of the same order of the integrin-to-integrin lateral separation observed experimentally [82] and one order of magnitude lower than the minimum separation between individual adhesions [86].

The probability of integrin deactivation is $P_d = k_d dt$. Once inactive, integrin loses its connections with ligands and other integrins. Integrins unbind ligands with dissociation probabilities depending on their affinities: $P = \lambda e^{E_{IL}} dt$, using a prefactor $\lambda = 1\ s^{-1}$, for simplicity. They break later connections with probabilities inversely proportional to strength of pairwise interaction: $P = \lambda e^{E_{II}} dt$. For β-1 integrins, we use high affinity, ~9 k_BT; for β-3 integrins we use lower affinity, 3–5 k_BT.

Ligand-bound integrins can establish harmonic interactions with semiflexible actin filaments below 5 nm, approximating the size of the intracellular integrin tails [82]. Since the exact molecular composition of the layer between integrin and actin can contain up to ~150 different proteins [87], a detailed modeling representation is not possible. Therefore, interactions between integrin and actin are approximated by harmonic potentials with equilibrium distance of 3 nm and spring constant of 1 pN/μm. These interactions simplify the ~40 nm layer of adhesion molecules, including vinculin, talin and α-actinin, and is consistent with the level of details of the simulations, where harmonic interactions are used to connect particles within 20–100 nm.

Brownian Dynamics simulations via the Langevin Equation

Displacements of integrin and actin filament particles are governed by the Langevin equation of motion in the limit of high friction, thus neglecting inertia:

$$\boldsymbol{F_i} - \xi_i \frac{d\boldsymbol{r}_i}{dt} + \boldsymbol{F}_i^T = 0 \tag{4}$$

where $\boldsymbol{r_i}$ is a position vector of the ith element, ζ_i is a drag coefficient equal in three directions, t is time, $\boldsymbol{F_i}$ is a deterministic force, and $\boldsymbol{F}_i^T$ is a stochastic force satisfying the fluctuation-dissipation theorem [88]. $\boldsymbol{F_i}$ is the sum of forces resulting from interactions of integrins with a ligand and/or other particles in the system, and actin flow in a direction parallel to the substrate. Positions of the various elements are updated at every time step using explicit Euler integration scheme:

$$\boldsymbol{r_i}(t + dt) = \boldsymbol{r_i}(\boldsymbol{t}) + \frac{1}{\xi_i}\left(\boldsymbol{F_i} + \boldsymbol{F}_i^T\right)dt \tag{5}$$

Integrin/ligand unbinding formalism

Since contraction forces are not needed for the assembly of nascent adhesions [5,10,89], our computational model only incorporates forces mimicking actin retrograde flow. In order to simulate actin flow and characterize distribution of traction stress at various flow rates, a constant force is applied on ligand bound integrins, along y (Fig 2B). Lifetime of the bond between integrin and ligand follows the catch-bond formalism (Fig 2C), using: for β-1 integrins an unloaded affinity of 2 s and a maximum lifetime of 15 s; for β-3 integrins an unloaded affinity of 0.5 s and a maximum lifetime of 3 s. The parameters for the catch bond kinetics are from previous experimental characterizations [38,47,56]. Curves of bond lifetime versus tension are shown in Fig 2C.

For β-1 integrins, we implemented an unbinding rate as a function of the force acting on the bond, F:

$$k_u(F) = 0.4\ e^{-0.04F} + 4E - 7\ e^{0.2F} \tag{6}$$

For β-3 integrins, we used unbinding rate:

$$k_u(F) = 2\ e^{-0.04F} + 4E - 6\ e^{0.2F} \tag{7}$$

The functional forms of the catch bonds were taken from a model that assumes a strengthening and a weakening pathway for the bond lifetimes, using a double exponential with exponents of opposite signs [90,91]. This model was also used for previous simulations of integrin-based adhesions [5].

Positive feedback between filament binding and integrin activation

To mimic promotion of integrin clustering upon ligand binding and actin filament engagement [81], we introduce a positive feedback between binding of integrin to a filament and integrin activation rate. In the model, integrins can bind a filament only if already bound to a ligand. Upon binding to actin, integrin activation rate is increased by 2 to 4% relative to its initial value. This assumption is motivated by recent evidence from TIRF experiments on T-cells, where it was demonstrated that actin binding and correct ligand positioning are needed for integrin activation [81]. The positive feedback between actin binding and integrin activation rate also represents conditions of inside-out signaling, with increased affinity for ligand binding induced by the cytoplasm [65]. We use the model with the positive feedback (schematics in Fig 2D) to test the effect of different actin architectures on ligand binding and clustering (Fig 6).

For bundled and crisscrossed actin filament architectures, we impose spatial restraints on filaments pairs. Bundled architectures have harmonic connections between beads of filament pairs that keep the filaments in parallel; crisscrossed architectures impose 90 deg angle between the axis of filaments pairs, that keep them almost perpendicular.

Experimental approach

Human Foreskin Fibroblasts (HFF) were purchased from ATCC and cultured in DMEM media (Mediatech) supplemented with 10% Fetal Bovine Serum (Corning), 2 mM L-glutamine (Invitrogen) and penicillin-streptomycin (Invitrogen). HFFs were plated on glass coverslips incubated with 10 μg/mL fibronectin (EMD Millipore) for 1 hr at room temperature. Cells were fixed 1 hr after plating by rinsing them in cytoskeleton buffer (10 mM MES, 3 mM $MgCl_2$, 1.38 M KCl and 20 mM EGTA) and then fixed, blocked and permeabilized in 4% PFA (Electron Microscopy Sciences), 1.5% BSA (Fisher Scientific), and 0.5% Triton X-100 (Fisher Scientific) in cytoskeleton buffer at 37˚ for 10 minutes. Coverslips were subsequently rinsed three times in PBS and incubated with either a β_1 antibody (1:100; Abcam product #:ab30394) or β_3 antibody (1:100; Abcam product #:ab7166) followed by AlexaFluor 488 phalloidin (1:1000; Invitrogen) and a AlexaFluor647 donkey anti-mouse secondary antibody (1:200; Invitrogen).

Cells were imaged using a 1.2 NA 60X Plan Apo water immersion lens on an inverted Nikon Ti-Eclipse microscope using an Andor Dragonfly spinning disk confocal system and a Zyla 4.2 sCMOS camera. The microscope was controlled using Andor's Fusion software.

Supporting information

S1 Fig. Integrin diffusivity cooperate with ligand density, strength of pairwise interactions, and affinity to mediate clustering and ligand binding. (A) Average fraction of clustered integrins and (B) corresponding fraction of ligand-bound integrins varying ligand density for two conditions of integrin properties: $D = 0.1\ \mu m^2/s$, $E_{IL} = 7\ k_BT$, $E_{II} = 9\ k_BT$; $D = 0.3\ \mu m^2/s$, $E_{IL} = 9\ k_BT$, $E_{II} = 9\ k_BT$. Data are computed between 80–100 s of simulations from three independent runs. (C) Average fractions of clustered and ligand-bound integrins varying diffusion coefficient, using $E_{IL} = 3\ k_BT$ and $E_{II} = 7\ k_BT$. Data are computed between 200–600 s of simulations, from three independent runs. (D) Average fractions of clustered and ligand-bound

integrins at $D = 0.1$ and 0.3 $\mu m^2/s$, $E_{IL} = 1\ k_BT$ and $E_{II} = 3\ k_BT$. Data are computed between 200–600 s of simulations, from three independent runs.
(TIF)

S2 Fig. Volume exclusion effects between integrins do not change ligand binding and traction stress as a function of actin flow. (A) Average fraction of ligand-bound integrins as a function of actin flow speed and percentage of β-1 integrins in a system of β-3 integrins. (B) Corresponding average nearest neighbor distance between ligand-bound integrins. (C) Corresponding average tension per integrin. (D) Distribution of tension on ligand-bound integrins for the two integrins types, using 80% β-1 and 20% β-3 integrins and 10 nm/s actin flow. Data are computed between 1–20 s of simulations, using a weak repulsive potential (1 pN) between integrins closer than 1 nm. Panels E-H show data as in panels A-D for implemented repulsive forces of 10 pN.
(TIF)

Author Contributions

Conceptualization: Tamara C. Bidone, Patrick W. Oakes, Gregory A. Voth.

Data curation: Tamara C. Bidone, Austin V. Skeeters.

Formal analysis: Tamara C. Bidone, Patrick W. Oakes.

Funding acquisition: Gregory A. Voth.

Methodology: Tamara C. Bidone, Gregory A. Voth.

Software: Tamara C. Bidone.

Supervision: Patrick W. Oakes, Gregory A. Voth.

Validation: Tamara C. Bidone.

Visualization: Austin V. Skeeters.

Writing – original draft: Tamara C. Bidone, Patrick W. Oakes.

Writing – review & editing: Patrick W. Oakes, Gregory A. Voth.

References

1. Ridley AJ. Cell Migration: Integrating Signals from Front to Back. Science (80-). 2003; 302: 1704–1709. https://doi.org/10.1126/science.1092053 PMID: 14657486
2. Webb DJ, Parsons JT, Horwitz AF. Adhesion assembly, disassembly and turnover in migrating cells–over and over and over again. Nat Cell Biol. 2002; 4: E97–E100. https://doi.org/10.1038/ncb0402-e97 PMID: 11944043
3. Geiger B, Yamada KM. Molecular architecture and function of matrix adhesions. Cold Spring Harb Perspect Biol. 2011; 3: 1–21. https://doi.org/10.1101/cshperspect.a005033 PMID: 21441590
4. Bachir AI, Horwitz AR, Nelson WJ, Bianchini JM. Actin-based adhesion modules mediate cell interactions with the extracellular matrix and neighboring cells. Cold Spring Harb Perspect Biol. 2017; 9. https://doi.org/10.1101/cshperspect.a023234 PMID: 28679638
5. Oakes PW, Bidone TC, Beckham Y, Skeeters AV, Ramirez-San Juan GR, Winter SP, et al. Lamellipodium is a myosin-independent mechanosensor. Proc Natl Acad Sci U S A. 2018; 115. https://doi.org/10.1073/pnas.1715869115 PMID: 29487208
6. Saltel F, Mortier E, Hytönen VP, Jacquier MC, Zimmermann P, Vogel V, et al. New PI(4,5)P2- and membrane proximal integrin-binding motifs in the talin head control β3-integrin clustering. J Cell Biol. 2009; 187: 715–731. https://doi.org/10.1083/jcb.200908134 PMID: 19948488

7. Cluzel C, Saltel F, Lussi J, Paulhe F, Imhof BA, Wehrle-Haller B. The mechanisms and dynamics of αvβ3 integrin clustering in living cells. J Cell Biol. 2005; 171: 383–392. https://doi.org/10.1083/jcb.200503017 PMID: 16247034
8. Ye F, Petrich BG, Anekal P, Lefort CT, Kasirer-Friede A, Shattil SJ, et al. The mechanism of kindlin-mediated activation of integrin??ilb??3. Curr Biol. 2013; 23: 2288–2295. https://doi.org/10.1016/j.cub.2013.09.050 PMID: 24210614
9. Paszek MJ, DuFort CC, Rossier O, Bainer R, Mouw JK, Godula K, et al. The cancer glycocalyx mechanically primes integrin-mediated growth and survival. Nature. 2014; 511: 319–325. https://doi.org/10.1038/nature13535 PMID: 25030168
10. Bachir AI, Zareno J, Moissoglu K, Plow EF, Gratton E, Horwitz AR. Integrin-associated complexes form hierarchically with variable stoichiometry in nascent adhesions. Curr Biol. 2014; 24: 1845–1853. https://doi.org/10.1016/j.cub.2014.07.011 PMID: 25088556
11. Coussen F, Choquet D, Sheetz MP, Erickson HP. Trimers of the fibronectin cell adhesion domain localize to actin filament bundles and undergo rearward translocation. J Cell Sci. 2002; 115: 2581–90. https://doi.org/10.1006/jmbi.1996.0137 PMID: 12045228
12. Shattil SJ, Kim C, Ginsberg MH. The final steps of integrin activation: the end game. Nat Rev Mol Cell Biol. 2010; 11: 288–300. https://doi.org/10.1038/nrm2871 PMID: 20308986
13. Bidone TC, Tang H, Vavylonis D. Dynamic network morphology and tension buildup in a 3D model of cytokinetic ring assembly. Biophys J. 2014; 107. https://doi.org/10.1016/j.bpj.2014.10.034 PMID: 25468341
14. Tang H, Bidone TC, Vavylonis D. Computational model of polarized actin cables and cytokinetic actin ring formation in budding yeast. Cytoskeleton. 2015; 72. https://doi.org/10.1002/cm.21258 PMID: 26538307
15. Bidone TC, Jung W, Maruri D, Borau C, Kamm RD, Kim T. Morphological Transformation and Force Generation of Active Cytoskeletal Networks. PLoS Comput Biol. 2017; 13. https://doi.org/10.1371/journal.pcbi.1005277 PMID: 28114384
16. Borau C, Kim T, Bidone T, Garcia-Aznar JM, Kamm RD. Dynamic mechanisms of cell rigidity sensing: insights from a computational model of actomyosin networks. PloS one. Aragon Institute of Engineering Research (I3A), Department of Mechanical Engineering, University of Zaragoza, Zaragoza, Spain.; 2012. p. e49174. https://doi.org/10.1371/journal.pone.0049174 PMID: 23139838
17. Zhang D, Bidone TC, Vavylonis D. ER-PM Contacts Define Actomyosin Kinetics for Proper Contractile Ring Assembly. Curr Biol. 2016; 26: 647–653. https://doi.org/10.1016/j.cub.2015.12.070 PMID: 26877082
18. Nayal A, Webb DJ, Brown CM, Schaefer EM, Vicente-Manzanares M, Horwitz AR. Paxillin phosphorylation at Ser273 localizes a GIT1-PIX-PAK complex and regulates adhesion and protrusion dynamics. J Cell Biol. 2006; 173: 587–599. https://doi.org/10.1083/jcb.200509075 PMID: 16717130
19. Vicente-Manzanares M, Zareno J, Whitmore L, Choi CK, Horwitz AF. Regulation of protrusion, adhesion dynamics, and polarity by myosins IIA and IIB in migrating cells. J Cell Biol. 2007; 176: 573–580. https://doi.org/10.1083/jcb.200612043 PMID: 17312025
20. Zaidel-Bar R. Early molecular events in the assembly of matrix adhesions at the leading edge of migrating cells. J Cell Sci. 2003; 116: 4605–4613. https://doi.org/10.1242/jcs.00792 PMID: 14576354
21. Changede R, Xu X, Margadant F, Sheetz MP, Critchley DR, Sheetz MP, et al. Nascent Integrin Adhesions Form on All Matrix Rigidities after Integrin Activation. Dev Cell. Elsevier; 2015; 35: 614–621. https://doi.org/10.1016/j.devcel.2015.11.001 PMID: 26625956
22. Zaidel-Bar R, Milo R, Kam Z, Geiger B. A paxillin tyrosine phosphorylation switch regulates the assembly and form of cell-matrix adhesions. J Cell Sci. 2006; 120: 137–148. https://doi.org/10.1242/jcs.03314 PMID: 17164291
23. Missirlis D, Haraszti T, Scheele C v. C, Wiegand T, Diaz C, Neubauer S, et al. Substrate engagement of integrins α5β1 and αvβ3 is necessary, but not sufficient, for high directional persistence in migration on fibronectin. Sci Rep. 2016; 6: 23258. https://doi.org/10.1038/srep23258 PMID: 26987342
24. Bunch TA. Integrin alphaIIb-beta3 activation in Chinese hamster ovary cells and platelets increases clustering rather than affinity. J Biol Chem. 2010; https://doi.org/10.1074/jbc.M109.057349 PMID: 19917607
25. Clyman RI, Mauray F, Kramer RH. Beta 1 and beta 3 integrins have different roles in the adhesion and migration of vascular smooth muscle cells on extracellular matrix. Exp Cell Res. 1992; https://doi.org/10.1016/0014-4827(92)90173-6
26. Hynes RO. Integrins: bidirectional, allosteric signaling machines. Cell. 2002; 110: 673–87. Available: http://www.ncbi.nlm.nih.gov/pubmed/12297042 PMID: 12297042

27. Laukaitis CM, Webb DJ, Donais K, Horwitz AF. Differential dynamics of??5 integrin, paxillin, and??-actinin during formation and disassembly of adhesions in migrating cells. J Cell Biol. 2001; 153: 1427–1440. https://doi.org/10.1083/jcb.153.7.1427 PMID: 11425873

28. Kiosses W, Shattil S, Pampori N, Schwartz M. Rac recruits high-affinity integrin αvβ3 to lamellipodia in endothelial cell migration. Nat Cell Biol. 2001; 3: 316–320. https://doi.org/10.1038/35060120 PMID: 11231584

29. Yee KO, Rooney MM, Giachelli CM, Lord ST, Schwartz SM. Role of beta1 and beta3 integrins in human smooth muscle cell adhesion to and contraction of fibrin clots in vitro. Circ Res. 1998; 83: 241–251. https://doi.org/10.1161/01.RES.83.3.241 PMID: 9710116

30. Legate KR, Takahashi S, Bonakdar N, Fabry B, Boettiger D, Zent R, et al. Integrin adhesion and force coupling are independently regulated by localized PtdIns(4,5) 2 synthesis. EMBO J. 2011; 30: 4539–4553. https://doi.org/10.1038/emboj.2011.332 PMID: 21926969

31. Wu X, Chakraborty S, Heaps CL, Davis MJ, Meininger GA, Muthuchamy M. Fibronectin increases the force production of mouse papillary muscles via??5??1 integrin. J Mol Cell Cardiol. 2011; 50: 203–213. https://doi.org/10.1016/j.yjmcc.2010.10.003 PMID: 20937283

32. Lin GL, Cohen DM, Desai RA, Breckenridge MT, Gao L, Humphries MJ, et al. Activation of beta 1 but not beta 3 integrin increases cell traction forces. FEBS Lett. 2013; 587: 763–769. https://doi.org/10.1016/j.febslet.2013.01.068 PMID: 23395612

33. Lu Z, Mathew S, Chen J, Hadziselimovic A, Palamuttam R, Hudson BG, et al. Implications of the differing roles of the β1 and β3 transmembrane and cytosplasmic domains for integrin function. Elife. 2016; https://doi.org/10.7554/eLife.18633 PMID: 27929375

34. Schultz JF, Armant DR. β1- and β3-class integrins mediate fibronectin binding activity at the surface of developing mouse peri-implantation blastocysts: Regulation by ligand-induced mobilization of stored receptor. J Biol Chem. 1995; https://doi.org/10.1074/jbc.270.19.11522 PMID: 7538116

35. Slepian MJ, Massia SP, Dehdashti B, Fritz A, Whitesell L. Beta3-integrins rather than beta1-integrins dominate integrin-matrix interactions involved in postinjury smooth muscle cell migration. Circulation. 1998; https://doi.org/10.1161/01.CIR.97.18.1818

36. Danen EHJ, Sonneveld P, Brakebusch C, Fässler R, Sonnenberg A. The fibronectin-binding integrins α5β1 and αvβ3 differentially modulate RhoA-GTP loading, organization of cell matrix adhesions, and fibronectin fibrillogenesis. J Cell Biol. 2002; https://doi.org/10.1083/jcb.200205014 PMID: 12486108

37. Elosegui-Artola A, Bazellières E, Allen MD, Andreu I, Oria R, Sunyer R, et al. Rigidity sensing and adaptation through regulation of integrin types. Nat Mater. 2014; https://doi.org/10.1038/nmat3960 PMID: 24793358

38. Roca-Cusachs P, Gauthier NC, Del Rio A, Sheetz MP. Clustering of alpha(5)beta(1) integrins determines adhesion strength whereas alpha(v)beta(3) and talin enable mechanotransduction. Proc Natl Acad Sci U S A. 2009; 106: 16245–16250. https://doi.org/10.1073/pnas.0902818106 PMID: 19805288

39. Jaqaman K, Galbraith JA, Davidson MW, Galbraith CG. Changes in single-molecule integrin dynamics linked to local cellular behavior. Mol Biol Cell. 2016; 27: 1561–1569. https://doi.org/10.1091/mbc.E16-01-0018 PMID: 27009207

40. Yu C -h., Law JBK, Suryana M, Low HY, Sheetz MP. Early integrin binding to Arg-Gly-Asp peptide activates actin polymerization and contractile movement that stimulates outward translocation. Proc Natl Acad Sci. 2011; 108: 20585–20590. https://doi.org/10.1073/pnas.1109485108 PMID: 22139375

41. Humphries JD, Wang P, Streuli C, Geiger B, Humphries MJ, Ballestrem C. Vinculin controls focal adhesion formation by direct interactions with talin and actin. J Cell Biol. 2007; 179: 1043–1057. https://doi.org/10.1083/jcb.200703036 PMID: 18056416

42. Galbraith CG, Yamada KM, Sheetz MP. The relationship between force and focal complex development. J Cell Biol. 2002; 159: 695–705. https://doi.org/10.1083/jcb.200204153 PMID: 12446745

43. Rossier O, Octeau V, Sibarita J-B, Leduc C, Tessier B, Nair D, et al. Integrins β1 and β3 exhibit distinct dynamic nanoscale organizations inside focal adhesions. Nat Cell Biol. 2012; 14: 1057–1067. https://doi.org/10.1038/ncb2588 PMID: 23023225

44. Li J, Su Y, Xia W, Qin Y, Humphries MJ, Vestweber D, et al. Conformational equilibria and intrinsic affinities define integrin activation. EMBO J. 2017; https://doi.org/10.15252/embj.201695803 PMID: 28122868

45. Lin ECK, Ratnikov BI, Tsai PM, Carron CP, Myers DM, Barbas CF, et al. Identification of a region in the integrin β3 subunit that confers ligand binding specificity. J Biol Chem. 1997; https://doi.org/10.1074/jbc.272.38.23912 PMID: 9295341

46. Zhao T, Li Y, Dinner AR. How focal adhesion size depends on integrin affinity. Langmuir. 2009; 25: 1540–1546. https://doi.org/10.1021/la8026804 PMID: 19132823

47. Friedland JC, Lee MH, Boettiger D. Mechanically Activated Integrin Switch Controls 5 1 Function. Science (80-). 2009; 323: 642–644. https://doi.org/10.1126/science.1168441 PMID: 19179533

48. García AJ, Huber F, Boettiger D. Force required to break??5??1 integrin-fibronectin bonds in intact adherent cells is sensitive to integrin activation state. J Biol Chem. 1998; 273: 10988–10993. https://doi.org/10.1074/jbc.273.18.10988 PMID: 9556578

49. Li F, Redick SD, Erickson HP, Moy VT. Force measurements of the alpha5beta1 integrin-fibronectin interaction. Biophys J. 2003; 84: 1252–1262. https://doi.org/10.1016/S0006-3495(03)74940-6 PMID: 12547805

50. Oakes PW, Beckham Y, Stricker J, Gardel ML. Tension is required but not sufficient for focal adhesion maturation without a stress fiber template. J Cell Biol. 2012; https://doi.org/10.1083/jcb.201107042 PMID: 22291038

51. Chan BM Rao A, Hemler ME. WJG. T cell receptor-dependent, antigen-specific stimulation of a murine T cell clone induces a transient, VLA protein-mediated binding to extracellular matrix. J Immunol. 1991;

52. Smith JW, Piotrowiczg RS, Mathis D, Piotrowicz RS. A mechanism for divalent cation regulation of beta 3-integrins. J Biol Chem. 1994;

53. Elices MJ, Urry LA, Hemler ME. Receptor functions for the integrin VLA-3: Fibronectin, collagen, and laminin binding are differentially influenced by ARG-GLY-ASP peptide and by divalent cations. J Cell Biol. 1991; https://doi.org/10.1083/jcb.112.1.169 PMID: 1986004

54. Shimaoka M, Takagi J, Springer TA. Conformational Regulation of Integrin Structure and Function. Annu Rev Biophys Biomol Struct. 2002; 31: 485–516. https://doi.org/10.1146/annurev.biophys.31.101101.140922 PMID: 11988479

55. Kong F, García AJ, Mould AP, Humphries MJ, Zhu C. Demonstration of catch bonds between an integrin and its ligand. J Cell Biol. 2009; https://doi.org/10.1083/jcb.200810002 PMID: 19564406

56. Li Y, Bhimalapuram P, Dinner AR. Model for how retrograde actin flow regulates adhesion traction stresses. J Phys Condens Matter. 2010; 22. https://doi.org/10.1088/0953-8984/22/19/194113 PMID: 21386439

57. Miyamoto S, Akiyama SK, Yamada KM. Synergistic roles for receptor occupancy and aggregation in integrin transmembrane function. Science (80-). 1995; https://doi.org/10.1126/science.7846531

58. Askari JA, Tynan CJ, Webb SED, Martin-Fernandez ML, Ballestrem C, Humphries MJ. Focal adhesions are sites of integrin extension. J Cell Biol. 2010; https://doi.org/10.1083/jcb.200907174 PMID: 20231384

59. Schaufler V, Czichos-Medda H, Hirschfeld-Warnecken V, Neubauer S, Rechenmacher F, Medda R, et al. Selective binding and lateral clustering of α5β1 and αvβ3 integrins: Unraveling the spatial requirements for cell spreading and focal adhesion assembly. Cell Adhesion and Migration. 2016. pp. 505–515. https://doi.org/10.1080/19336918.2016.1163453 PMID: 27003228

60. Gardel ML, Sabass B, Ji L, Danuser G, Schwarz US, Waterman CM. Traction stress in focal adhesions correlates biphasically with actin retrograde fl ow speed. J Cell Biol. 2008; 183: 999–1005. https://doi.org/10.1083/jcb.200810060 PMID: 19075110

61. Craig EM, Stricker J, Gardel M, Mogilner A. Model for adhesion clutch explains biphasic relationship between actin flow and traction at the cell leading edge. Phys Biol. 2015; 12. https://doi.org/10.1088/1478-3975/12/3/035002 PMID: 25969948

62. Cavalcanti-Adam EA, Volberg T, Micoulet A, Kessler H, Geiger B, Spatz JP. Cell Spreading and Focal Adhesion Dynamics Are Regulated by Spacing of Integrin Ligands. Biophys J. 2007; 92: 2964–2974. https://doi.org/10.1529/biophysj.106.089730 PMID: 17277192

63. Nordenfelt P, Elliott HL, Springer TA. Coordinated integrin activation by actin-dependent force during T-cell migration. Nat Commun. 2016; 7. https://doi.org/10.1038/ncomms13119 PMID: 27721490

64. Galbraith CG, Yamada KM, Galbraith JA. Polymerizing Actin Fibers Position Integrins Primed to Probe for Adhesion Sites. Science (80-). 2007; 315: 992–995. https://doi.org/10.1126/science.1137904 PMID: 17303755

65. Vinogradova O, Velyvis A, Velyviene A, Hu B, Haas TA, Plow EF, et al. A structural mechanism of integrin αIIbβ3"inside-out" activation as regulated by its cytoplasmic face. Cell. 2002; https://doi.org/10.1016/S0092-8674(02)00906-6

66. Chen W, Lou J, Hsin J, Schulten K, Harvey SC, Zhu C. Molecular Dynamics Simulations of Forced Unbending of Integrin αVβ3. Paci E, editor. PLoS Comput Biol. 2011; 7: e1001086. https://doi.org/10.1371/journal.pcbi.1001086 PMID: 21379327

67. Jin M, Andricioaei I, Springer TA. Conversion between three conformational states of integrin I domains with a C-terminal pull spring studied with molecular dynamics. Structure. 2004; https://doi.org/10.1016/j.str.2004.10.005 PMID: 15576028

68. Pagani G, Gohlke H. On the contributing role of the transmembrane domain for subunit-specific sensitivity of integrin activation. Sci Rep. 2018; https://doi.org/10.1038/s41598-018-23778-5 PMID: 29636500

69. Kalli AC, Campbell ID, Sansom MSP. Multiscale simulations suggest a mechanism for integrin inside-out activation. Proc Natl Acad Sci. 2011; https://doi.org/10.1073/pnas.1104505108 PMID: 21730166

70. Kalli AC, Rog T, Vattulainen I, Campbell ID, Sansom MSP. The Integrin Receptor in Biologically Relevant Bilayers: Insights from Molecular Dynamics Simulations. J Membr Biol. 2017; https://doi.org/10.1007/s00232-016-9908-z PMID: 27465729

71. Gaillard T, Dejaegere A, Stote RH. Dynamics of β3 integrin I-like and Hybrid domains: Insight from simulations on the mechanism of transition between open and closed forms. Proteins Struct Funct Bioinforma. 2009; https://doi.org/10.1002/prot.22404 PMID: 19350618

72. Paszek MJ, Boettiger D, Weaver VM, Hammer DA. Integrin clustering is driven by mechanical resistance from the glycocalyx and the substrate. PLoS Comput Biol. 2009; 5. https://doi.org/10.1371/journal.pcbi.1000604 PMID: 20011123

73. Lepzelter D, Zaman MH. Clustered diffusion of integrins. Biophys J. 2010; https://doi.org/10.1016/j.bpj.2010.11.007 PMID: 21156122

74. Bidone TC, Polley A, Jin J, Driscoll T, Iwamoto D V., Calderwood DA, et al. Coarse-Grained Simulation of Full-Length Integrin Activation. Biophys J. 2019; https://doi.org/10.1016/j.bpj.2019.02.011 PMID: 30851876

75. Irvine DJ, Hue KA, Mayes AM, Griffith LG. Simulations of cell-surface integrin binding to nanoscale-clustered adhesion ligands. Biophys J. 2002; https://doi.org/10.1016/S0006-3495(02)75379-4 PMID: 11751301

76. Brinkerhoff CJ, Linderman JJ. Integrin Dimerization and Ligand Organization: Key Components in Integrin Clustering for Cell Adhesion. Tissue Eng. 2005; https://doi.org/10.1089/ten.2005.11.865 PMID: 15998226

77. Welf ES, Naik UP, Ogunnaike BA. A spatial model for integrin clustering as a result of feedback between integrin activation and integrin binding. Biophys J. 2012; https://doi.org/10.1016/j.bpj.2012.08.021 PMID: 22995511

78. Lepzelter D, Bates O, Zaman M. Integrin clustering in two and three dimensions. Langmuir. 2012; https://doi.org/10.1021/la203725a PMID: 22204631

79. Nedelec F, Foethke D. Collective Langevin dynamics of flexible cytoskeletal fibers. New J Phys. 2007; https://doi.org/10.1088/1367-2630/9/11/427

80. Popov K, Komianos J, Papoian GA. MEDYAN: Mechanochemical Simulations of Contraction and Polarity Alignment in Actomyosin Networks. PLoS Comput Biol. 2016; https://doi.org/10.1371/journal.pcbi.1004877 PMID: 27120189

81. Nordenfelt P, Elliott HL, Springer TA. Coordinated integrin activation by actin-dependent force during T-cell migration. Nat Commun. 2016; 7: 13119. https://doi.org/10.1038/ncomms13119 PMID: 27721490

82. Xu X-P, Kim E, Swift M, Smith JW, Volkmann N, Hanein D. Three-Dimensional Structures of Full-Length, Membrane-Embedded Human α(IIb)β(3) Integrin Complexes. Biophys J. The Biophysical Society; 2016; 110: 798–809. https://doi.org/10.1016/j.bpj.2016.01.016 PMID: 26910421

83. Tang H, Laporte D, Vavylonis D. Actin cable distribution and dynamics arising from cross-linking, motor pulling, and filament turnover. Mol Biol Cell. 2014; 25: 3006–3016. https://doi.org/10.1091/mbc.E14-05-0965 PMID: 25103242

84. Pasquali M, Shankar V, Morse DC. Viscoelasticity of dilute solutions of semiflexible polymers. Phys Rev E—Stat Nonlinear, Soft Matter Phys. 2001; 64: 208021–208024. https://doi.org/10.1103/PhysRevE.64.020802 PMID: 11497554

85. Kojima H, Ishijima A, Yanagida T. Direct measurement of stiffness of single actin filaments with and without tropomyosin by in vitro nanomanipulation. Proc Natl Acad Sci U S A. 1994;

86. Stricker J, Aratyn-Schaus Y, Oakes PW, Gardel ML. Spatiotemporal constraints on the force-dependent growth of focal adhesions. Biophys J. 2011; 100: 2883–2893. https://doi.org/10.1016/j.bpj.2011.05.023 PMID: 21689521

87. Zaidel-Bar R, Itzkovitz S, Ma'ayan A, Iyengar R, Geiger B. Functional atlas of the integrin adhesome. Nat Cell Biol. 2007; https://doi.org/doi:10.1038/ncb0807-858

88. Underhill PT, Doyle PS. On the coarse-graining of polymers into bead-spring chains. J Nonnewton Fluid Mech. 2004; 122: 3–31. https://doi.org/10.1016/j.jnnfm.2003.10.006

89. Choi CK, Vicente-Manzanares M, Zareno J, Whitmore LA, Mogilner A, Horwitz AR. Actin and α-actinin orchestrate the assembly and maturation of nascent adhesions in a myosin II motor-independent manner. Nat Cell Biol. Nature Publishing Group; 2008; 10: 1039–1050. https://doi.org/10.1038/ncb1763 PMID: 19160484

90. Pereverzev Y V., Prezhdo O V., Thomas WE, Sokurenko E V. Distinctive features of the biological catch bond in the jump-ramp force regime predicted by the two-pathway model. Phys Rev E—Stat Nonlinear, Soft Matter Phys. 2005; https://doi.org/10.1103/PhysRevE.72.010903 PMID: 16089930

91. Pereverzev Y V., Prezhdo O V., Forero M, Sokurenko E V., Thomas WE. The two-pathway model for the catch-slip transition in biological adhesion. Biophys J. 2005; https://doi.org/10.1529/biophysj.105.062158 PMID: 15951391